

Study of the Erosive-abrasive Wear Resistance of Fe-14%Cr-2.8%C High Chromium Cast Iron

Adonias Ribeiro Franco Júnior^{a*} , Jaime Alberto Sanchez Caceres^a , Diego Loubach da Rocha^a

^aInstituto Federal do Espírito Santo, Vitória, ES, Brasil.

Received: May 16, 2023; Revised: November 08, 2023; Accepted: November 27, 2023

High chromium cast irons (HCCIs) are widely applied in the mining industry as components of equipment for iron ore transportation, in which their surfaces are subjected to abrasive and erosive wear. The present work evaluated the erosion-abrasion behavior of a HCCI possessing different amounts of austenite and martensite, using a laboratory impeller-tumbler wear test apparatus and iron ore pellets as abrasive material. The results showed that the wear dominant mechanism on the worn surface of the as-cast material depends upon the material microstructure. For HCCI destabilized at 930 and 990 °C, the matrix has high martensite/austenite ratio and finely dispersed secondary carbides, offering high abrasion-erosion wear resistance. The absence of fractured eutectic carbides indicates that such matrix has hardness and load bearing capacity, enough for mitigating a significant plastic deformation during the impact pellets. For HCCI destabilized at 1050 °C, the matrix has a low martensite/austenite ratio and coalesced secondary carbides, leading to high wear rates during erosion-abrasion tests.

Keywords: *high chromium cast iron, austenite destabilization, martensite/austenite ratio, impeller-tumbler test.*

1. Introduction

The loss occasioned by the wear results in high maintenance costs for equipment used in various industry segments. An example is the wear of plates applied in iron ore transport systems as sacrificial elements which usually undergo wear not only by abrasion, but also by erosion. The latter occurs when the ore particles impinge on the surface of the plates at relatively high speeds and high angles, close to 90°, while the first is caused by the sliding of such particles against the material surface. In general, erosion is localized whilst abrasion tends to be more evenly distributed¹.

The most commonly used materials in such application are tough, wear- and abrasion-resistant, high chromium cast iron (HCCI) alloys with as-cast microstructure consisting of eutectic carbides in a metastable austenitic matrix. Some works have shown that an improved abrasive wear resistance is attained by the heat treatment of destabilization^{2,3}, either by increasing the volume fraction of martensite or from the precipitation of secondary carbides^{4,6}. During the soaking period, the precipitation of secondary carbides promotes the depletion of alloying elements and, as a result, the austenite destabilization³⁻⁷. A rapid cooling performed immediately after the destabilization usually leads to large amounts of martensite and the resulting hardened matrix provides greater support for the carbides, which can locally block the evolution of wear⁶⁻⁸.

The laboratory wear tests for assessing and understanding the wear mechanisms acting at the material/abrasive contact are crucial for the development of technologies and new materials, which consequently can lead to a reduction in costs associated with downtime for component maintenance or replacement⁹.

The objective of the present work was to analyze the erosion-abrasion wear behavior of a hypo-eutectic high chromium cast iron (HCCI), destabilized at different temperatures, using a laboratory impeller-tumbler wear test apparatus, loaded with iron ore pellets (abrasive). Experiments conducted by Kirchgaßner et al.¹⁰ have demonstrated that using such wear test setup, as well as the size and weight of the abrasive particles, the impact produced by the abrasive particles on the specimens will possess enough high energy to cause the erosion wear, in addition to the abrasion.

2. Experimental Procedure

2.1. Material characterization and destabilization conditions

The material used in the present investigation, manufactured by a regional company, was provided by Vale S.A. in the form of plates measuring 600 × 600 × 75 mm, and hardness of 42 HRC. Using Oxford optical emission spectrometer (OES), model Foundry-Master Pro, the following chemical composition was determined (in wt.%): C=2.80, Cr=13.56, Si=0.97, Mn=0.88, Ni=0.26, Mo=0.76, P=0.058, S=0.026 and Fe= bal. Considering the contents found for C and Cr, the alloy can be classified as hypoeutectic high chromium cast iron (HCCI) Class-II Type-A, according to the ASTM A532 standard.

Rectangular specimens measuring approximately 70 mm × 35 mm × 25 mm were cut using water-jet cutting from the plates. Using an electrical resistance furnace with an argon atmosphere to prevent oxidation, the heat treatment involved pre-heating up to 650 °C and 1 h, destabilization at three different temperatures (930 °C, 990 °C 1050 °C),

*e-mail: adonias.franco@ifes.edu.br

soaking time of 1h, and cooling in air. The surface of the specimens was ground with SiC paper (#120, 200 and 400 grits) to remove oxide layers.

After grinding, polishing and etching with Vilella's reagent, the HCCI samples were characterized using a light microscope Leica model 750 DM and by a scanning electron microscope (SEM) Zeiss model EVO MA10 Collection was performed using a voltage of 25 kV, in secondary electron detection mode on the SE1 detector. X-ray analyses were performed using a Bruker mod D2 Phaser diffractometer equipped with CuK α radiation ($K\alpha$ - λ =0.154 nm), graphite monochromator, voltage of 30 kV in continuous scanning mode, varying 2θ in the range of 10 to 100°.

JMat-Pro simulation software was used to determine the carbon and chromium content in austenite. The amount of carbides and the amount secondary carbides were determined using the ImageJ software installed in the light microscope, while austenite and martensite were quantified according to ASTM-E975-13 standard¹¹, calculating the area under the X-rays peaks using the Origin Pro 2018 software.

Hardness measurements were carried out according to NM ISO 6508-1/2016 standard, by using a Heckert Rockwell hardness tester with a load of 150 gf/mm².

2.2. Impeller-tumbler test procedure

The erosive-abrasive wear resistance of the HCCI specimens possessing different amounts of martensite was assessed using an impeller-tumbler tribometer, whose constructive details are shown elsewhere^{12,13}. Figure 1 schematically shows the test setup, where up to three specimens, held in slots of the impeller, can be tested. Spherically shaped iron ore pellets ranging in diameter from 8 to 13 mm were used as abrasive material in order to obtain similarity with the actual conditions found in the mining industry. The wear of the specimens will occur due to the impact with the abrasive,

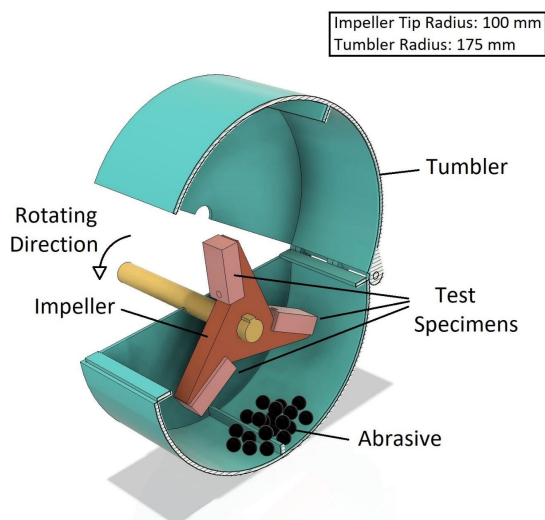


Figure 1. Schematic of the impeller-tumbler tribometer used in the erosion-abrasion wear tests.

which is impelled at a high energy generated by the impeller rotating at a speed of 700 RPM, resulting in an impact velocity of 7.33 m/s at the tip of the specimens. For each condition three specimens were tested twice, considering both sides, resulting in six measurements. The erosion-abrasion test duration was approximately 4 h and the values of weight loss were determined with accuracy of ± 1 mg by weighing the specimens every 20 min during the first hour, and then every 1 hour of testing. During weighing procedure, the load of partially-fractured pellets was replaced by a new load, and the specimens were re-fixed in the impeller slots at positions different from the previous ones, to ensure test reproducibility. To eliminate the abrasive, the surfaces of the specimens were subjected to the steps of rinsing and brushing under running water, agitation in ultrasonic bath, and drying with hot air. The material structures both on the surface and below the wear track were analyzed by SEM after deep-etching.

3. Results and Discussion

3.1. Microstructures of HCCI in as-cast condition and destabilized

Figure 2 shows the phases identified in the microstructure of HCCI as-received and destabilized at temperatures of 930 °C, 990 °C and 1050 °C. It is noted that martensite, austenite and carbides are evidenced in all the microstructural conditions.

The XRD results confirm the presence of expected microconstituents for the type of HCCI and serve as a basis for determining the volumetric fractions of austenite and martensite.

In this case, the peaks selected in the diffractogram of Figure 2 are those coming from plane 220 generated by angle $2\theta=74.48^\circ$, which corresponds to the austenite phase, and the peak of plane 200 generated by angle $2\theta=64.89^\circ$, which corresponds to phase martensite.

They were selected because they did not show interference from peaks from other phases, such as the most expressive peaks of index 2 and 3 located in the range of 42 to 46°.

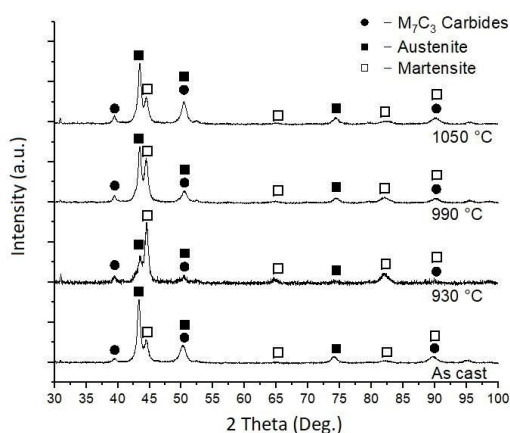


Figure 2. X-ray diffraction patterns for HCCI as-cast and destabilized at 930 °C, 990 °C and 1050 °C.

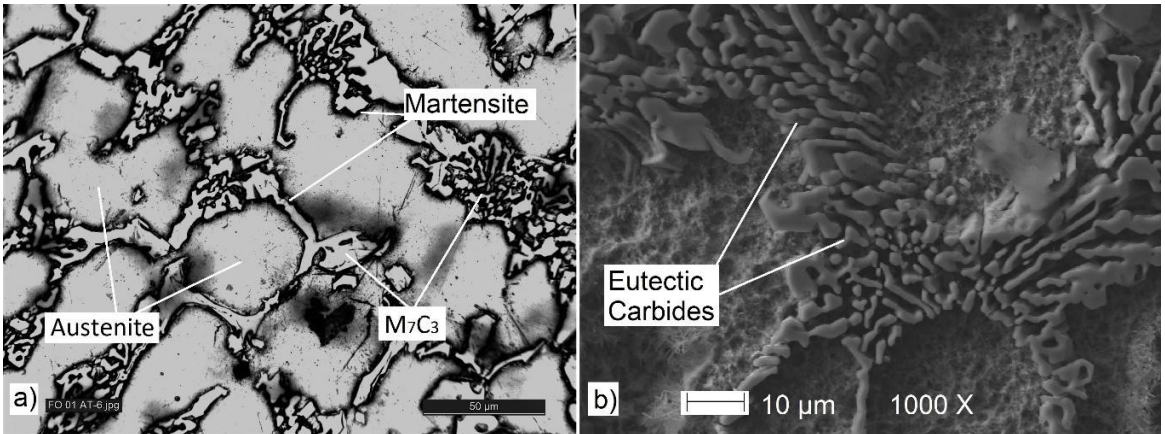


Figure 3. Microstructure of the as-cast HCCI after: (a) Vilella etching, and (b) deep etching.

The quantification performed provided a result of 45% austenite, which confirms satisfactorily the results presented so far.

XRD analyzes made it possible to highlight the changes microstructural resulting from heat treatments. In the diffractograms shown in Figure 2, it is possible to notice the occurrence of changes in the intensities of the peaks corresponding to austenite and martensite, present in the matrix.

As shown in Figure 2, the peaks with the most significant intensity variations are those corresponding to 2θ of 44° (austenite) and 46° (martensite).

The contents of carbon dissolved in austenite obtained for the temperatures 930°C , 990°C and 1050°C were 0.63% C, 0.74 and 0.87% C, respectively. We can affirm that with the use of higher destabilization temperatures, such as 1050°C , martensite with higher carbon content is likely to form during cooling. Figure 3a shows the as-cast microstructure of the HCCI, where we can see the austenite matrix (clear areas) and the eutectic microconstituent, which is consisted of alternating layers of M_7C_3 carbides, according Figure 2, and austenite (matrix). In the solidification, austenite dendrites are first formed and then the eutectic microconstituent after reaching the eutectic temperature. Next to the interfaces between eutectic carbide and austenite matrix, the presence of martensite (dark areas), favored by the depletion of carbon and alloying elements in austenite, is also evidenced. Such depletion increases the martensite-start temperature (M_s), so that the formation of martensite with high hardness is favored^{5,7}. Figure 3b shows that the carbides are interconnected to the austenite matrix, and they possess a bar-like morphology, similar to those found by Bedolla-Jacuinde et al.⁴.

The amount of identified phases is presented in Figure 4. It is to be noted that the volume fractions of carbides for the destabilized material are lower than those for the as-cast material, suggesting that their partial dissolution may have occurred during destabilization. High volume fractions of martensite were produced at destabilization temperature of 930°C and, increasing the temperature up to 1050°C led to a progressive decrease in the volume fraction of martensite, resulting in martensite quantum close to those for the as-cast material.

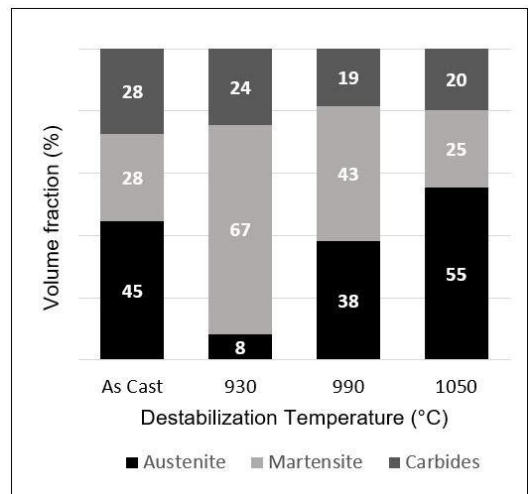


Figure 4. Volume fraction of microconstituents in HCCI destabilized at different temperatures.

Figure 5 shows the microstructures of the HCCI after destabilization at 930°C , 990°C and 1050°C , and air cooling. Significant microstructural changes are observed when the as-cast microstructure, Figure 3, is compared with the destabilized ones, Figure 5a-c.

For the 930°C -destabilized microstructure, we can observe that fine secondary carbides appear dispersed and distributed along the entire austenite matrix. This is because the lower the temperature, the more nucleation sites will appear, and, consequently, the resultant microstructure will possess finely dispersed secondary carbides. Also, martensite islands were formed in the austenite matrix.

At temperature of 990°C , Figure 5b, it can be seen that the secondary carbides are coarser than those found in the microstructure of the destabilized material at a temperature of 930°C . As the temperature is high, the nucleation frequency of these carbides is probably lower, as well as the beginning of its precipitation. However, the increase in temperature also has the effect of coalescing the small carbides close together, making them more visible under the microscope.

Bedolla-Jacuinde et al.⁴ found a small fraction of secondary carbides formed using lower destabilization temperatures. Austenite has a lower carbon and chromium retention capacity and therefore a greater volume of secondary carbides is expected. However, the precipitation kinetics varies with the destabilization temperature. At temperatures below 990 °C, a longer soaking time is required for complete precipitation. These authors obtained a high fraction of secondary carbides for treatment at lower temperatures only with soaking times longer than three hours. In the present work, soaking times of one hour were used, which suggests that there was not enough time for complete precipitation at a temperature of 930 °C.

For the 1050 °C–destabilized microstructure, unlike the carbides, the visualization of martensite became more difficult. Increasing temperatures, therefore, led to the coalescence of carbides. Large globular carbides are formed as a result of the coalescence phenomenon that occurs markedly in this temperature range according to Bedolla-Jacuinde et al.⁴.

3.2. Relationship among hardness, martensite/austenite ratio, and resistance to erosive-abrasive wear

For the HCCI in as-cast condition and destabilized at different temperatures, Figure 6 shows the variations in both the volume fraction of martensite and the bulk hardness.

It should be noted in Figure 6 that increased amounts of martensite led to a significant increase in the hardness. The maximum values for hardness (~59.8 HRC) and for volume fraction of martensite (67%) were attained when the material is destabilized at 930 °C. In this condition, the material contains only 8% of austenite as shown in Figure 4. According to Karantzalis et al.³, HCCIs with similar proportions of microconstituents can exhibit an optimal combination of strength and toughness. Additionally, the presence of secondary carbides, finely dispersed in a high hardness matrix, can improve the wear resistance, due to their hardening effect.

In contrast, increasing the temperature up to 990 °C, both the fraction of martensite and hardness decreased to 43% and 50.0 HRC, respectively. A more significant reduction is experienced by the 1050 °C destabilized samples, which possess hardness and martensite fraction very close to the as-cast samples. Therefore, it is inferred that the HCCI hardness is dependent on the volume fraction of martensite. Increasing the destabilization temperature, a downward displacement of both M_s and M_f temperature occurs due to the increase of carbon content in austenite, which makes its transformation into martensite difficult⁴.

Figure 7 shows the mass loss after impeller-tumbler wear tests. It is noticed that for all microstructural conditions, during the first hour of test, there is a running-in period where the wear rate is high at the initial stage (till about 1 h). This shows that the permanent regime can be achieved in a short period. Possibly, high wear rates are associated with an intense plastic deformation experienced by the worn surface at the initial stage due to the first impacts suffered at the running-in period¹⁴. In the first 60 min, the samples showed more pronounced wear, where the still intact surfaces of the samples suffer penetrations and scratching caused by the abrasives and some abrasive particles detached from the abrasives incorporate the surface, making the geometry of the samples more rounded. Similar results were found by Ratia et al.¹² and Wilson and Hawk¹⁴.

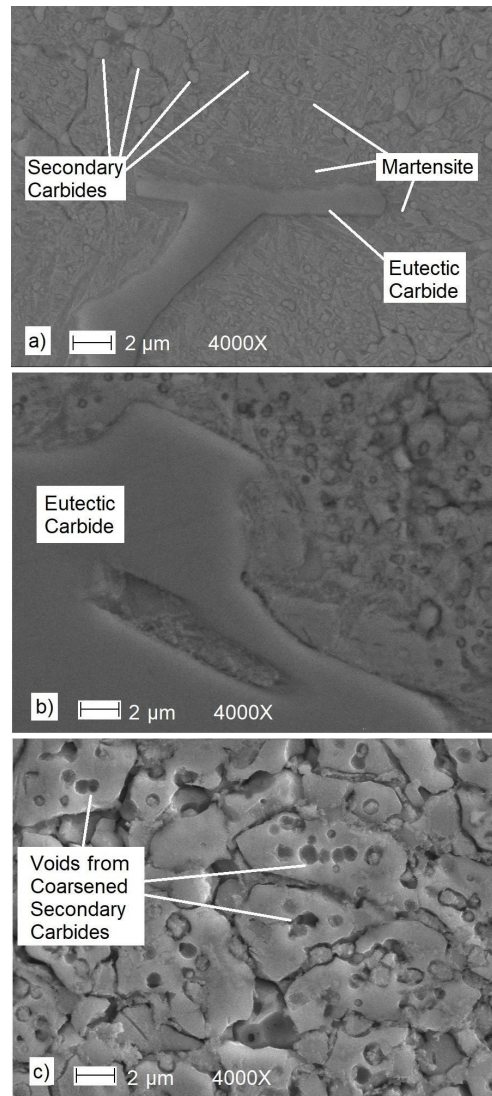


Figure 5. Microstructures of the FFAC after destabilization performed at: (a) 930 °C (martensite and secondary carbides); (b) 990 °C (martensite surrounding the eutectic carbides); (c) 1050 °C (coalesced secondary carbides).

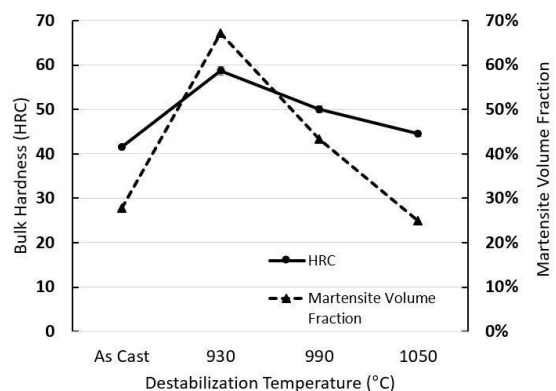


Figure 6. Variation of hardness and martensite fraction for HCCI as a function of microstructural condition.

Figure 8 shows the variations of wear rate (g/h) as a function of test duration for different microstructural conditions studied in this work. It should be noted that the erosion-abrasion behavior is strongly dependent on the microstructural condition. The wear rate for 930 °C-destabilized samples is lower, in comparison to other samples. This microstructural condition possesses 67% of martensite and 59.8 HRC, besides a fine dispersion of secondary carbides as observed in Figure 5a. According to Xu et al.⁹, such a microstructure provides more effective blocking of the dislocation movement, restricting the plastic deformation and, consequently, the wear losses.

For the material samples under different microstructural conditions after wear tests, Figure 9 shows the cross sections just below the worn surface.

For the as-cast material, one can see that in the upper portion of Figure 9a, b both intense plastic deformation of the matrix and fractures of eutectic carbide occurred from the surface towards distant regions. Therefore, extensive plastic deformation is due to the matrix not being hard enough to withstand the high strain rates imposed on the material surface by the impacts.

The material surfaces destabilized at 930 °C, Figure 9c, d, have a predominantly martensitic matrix and therefore exhibited more plastic deformation resistance. Unlike the as-cast material, no deformation occurs in either the matrix or worn edges (upper part). The presence of finely-dispersed secondary carbides in the matrix mitigated the grooving process due to their blocking effect. However, in regions near the worn surfaces, some fractures of eutectic carbides are also noted. These fractures are limited to regions very close to the surface, leading to the detachment of more carbides. A very hard martensite matrix containing very fine carbide dispersion, therefore, provides a high erosion-abrasion resistance to the material.

In the samples destabilized at 1050 °C, Figure 9e, f, the plastic deformation of the matrix was limited to the edge (upper part of the images). However, as well in the as-cast material, the process of eutectic carbide fracture reached great depths. This indicates that the matrix with coarse carbides does not offer enough support for carbides. As shown in Figure 7, the material wear rate is similar to that of the as-cast ones, which has equally close amounts of martensite and austenite (Figure 4).

Figure 10 shows the worn surfaces after the erosion-abrasion wear tests. For all these surfaces, microfractures which resulted from successive impacts of the pellets and consequent detachment of material are observed.

From Figure 10a, one can infer that the material removal occurred predominantly through microfractures at the plastically deformed areas due to both the successive impacts (erosion) and, to a lesser extent, the abrasion. The wear behavior of the as-cast structure is related to the high amount of austenite and the absence of visible secondary carbides in the matrix.

The sample destabilized at 930 °C, Figure 10b, exhibited the lowest wear rate. The structure containing a high hardness matrix became difficult for the penetration of the abrasive particles. Additionally, the presence of secondary carbides with high adhesion to the matrix interrupted the particles sliding over long distances, mitigating the wear losses.

For 990 °C destabilized sample, Figure 10c, the worn surface presented an intermediated wear resistance, or rather, its wear resistance is superior to that of as-cast sample and inferior to the sample destabilized at 930 °C. This behavior, as shown in Figure 7, is attributed to the decrease in the volume fraction of martensite.

The 1050 °C-destabilized sample, Figure 10d, exhibited the highest wear rate as shown in Figure 7. The advancement of the wear was facilitated by the presence of coalesced secondary carbides that are easily pulled out (low cohesion) during impact. Similarly, for the as-cast matrix, a low hardness matrix contributed to the fracture of eutectic carbides, due to the low martensite/austenite ratio.

Figure 11 shows the obtained results for the volume fraction of secondary carbides precipitated for 1 hour of soaking for each of the studied temperatures. At 930 °C, it was observed volume fraction of 13%, this occurs due to the diffusion process of chromium and carbon.

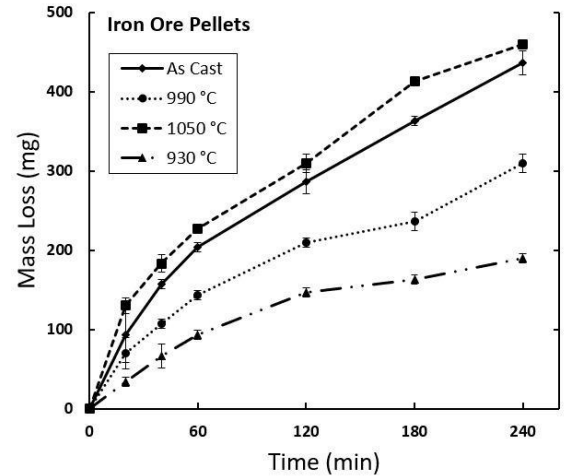


Figure 7. Variation of the mass loss during erosion-abrasion test in an impeller-tumbler tribometer for HCCI as-cast and destabilized at different temperatures. Abrasive used: iron ore pellets.

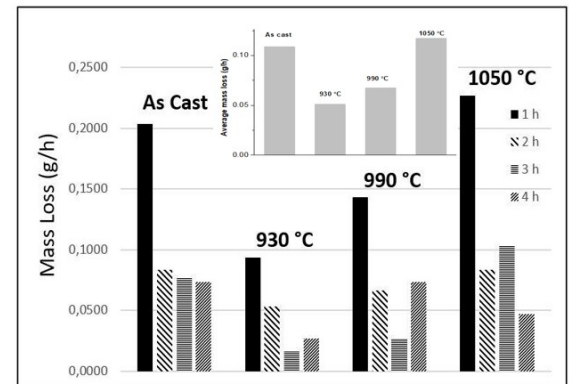


Figure 8. Variation of the wear rate during erosion-abrasion test in an impeller-tumbler tribometer as a function of test duration, for HCCI as-cast and destabilized at different temperatures and average wear rates at between 1h e 4 h. Abrasive used: iron ore pellets.

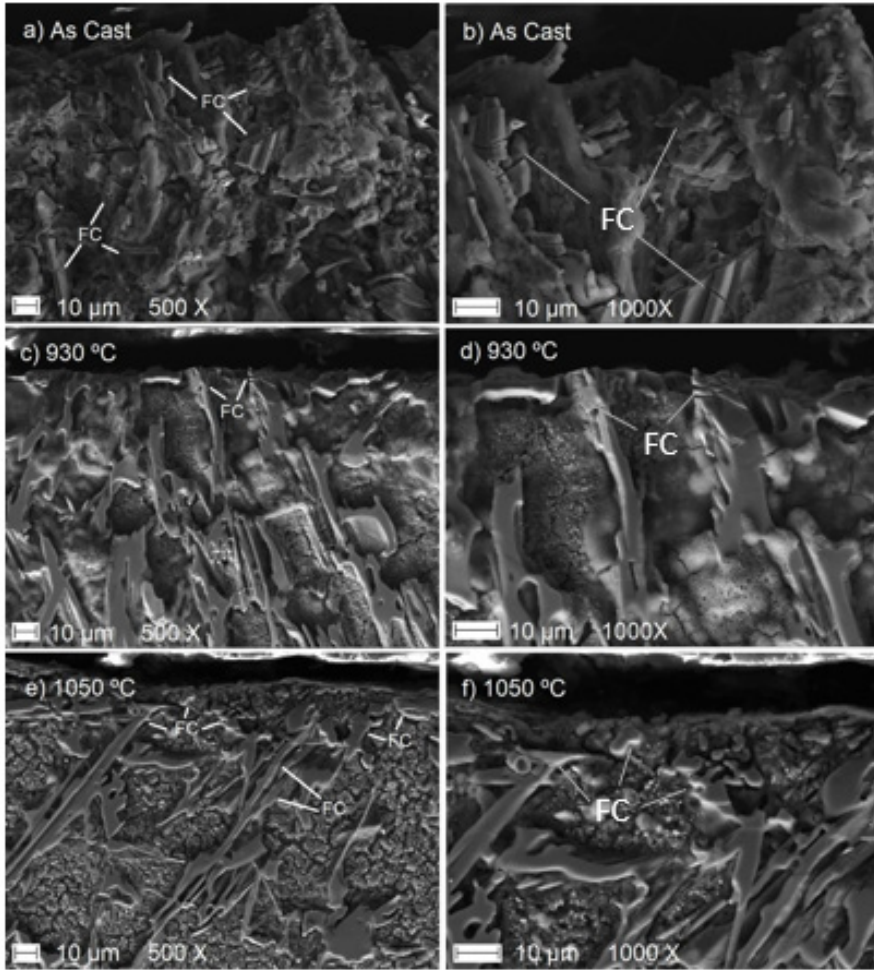


Figure 9. SEM of cross section of the worn surfaces after impeller-tumbler tests. The areas exposed to wear are on the top of the pictures. Obs.: FC – Fractures on the carbides.

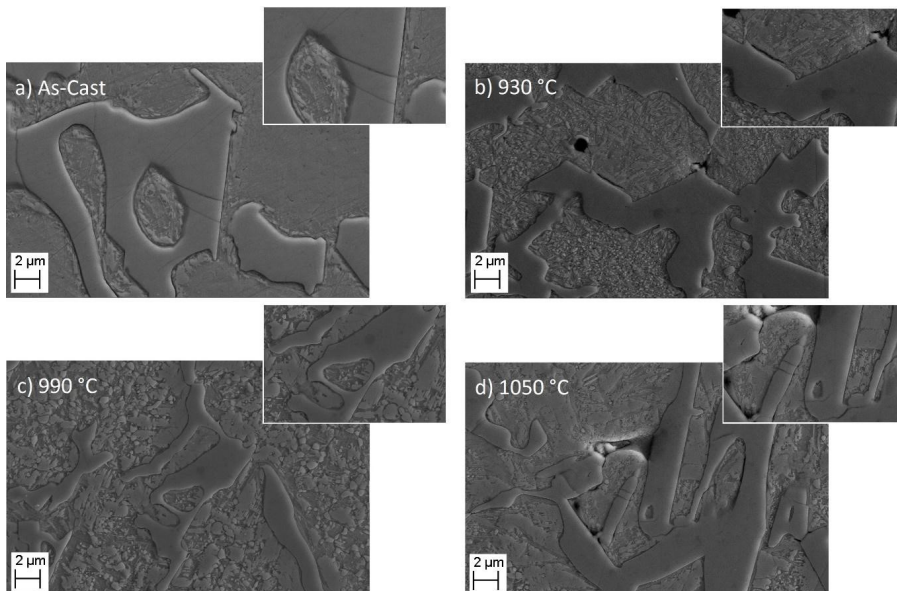


Figure 10. Worn surfaces after 4 hour-impeller-tumbler testing and etching. The marked areas correspond to 2X magnification.

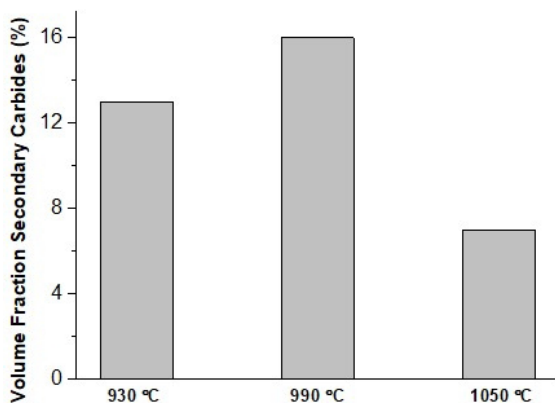


Figure 11. Volume fraction secondary carbides in HCCI destabilized at different temperatures.

At 990 °C the total volume fraction precipitated of secondary carbides was 16%. Higher temperatures, near 1000 °C, accelerated the process due to the higher diffusion rate of the elements that form the carbides secondary, chromium, and carbon.

At 1050 °C a volume fraction of 7% at 1 h soaking. At high temperatures the diffusion rates for chromium and carbon are higher, however at this temperature the precipitation of secondary carbides decreases. This behavior can be explained due the initial amount of carbides had precipitated during heating to the soaking temperature and these carbides dissolving during soaking time.

4. Conclusions

For high chromium cast iron (HCCI) 14% Cr-2.8% C, it can be concluded that after destabilization heat treatments in the range of 930-1050 °C and air cooling, and erosion-abrasion wear tests in the impeller-tumbler using iron ore pellets as abrasive:

- i. Destabilization temperatures between 930 and 990 °C provide a HCCI microstructure containing larger martensite fractions and a fine dispersion of secondary carbides, which led to significant reduction in the abrasive- erosive wear coefficient in comparison with the as-cast material.
- ii. Low hardness matrix contributed to the fracture of eutectic carbides due to the low martensite/austenite ratio, and, consequently, to more wear losses.
- iii. The predominant wear mechanisms are influenced by the matrix microstructure. For the as-cast or 1050 °C-destabilized HCCL, abrasion plays an important role due to the high-volume fraction austenite and the presence of coarse secondary carbides.
- iv. The wear resistance is lowered when the microstructure matrix has a low hardness and, consequently, offers both low abrasion resistance and eutectic carbide support. Additionally, the presence of coalesced secondary carbides has a deleterious effect, because they are easily detached during the impact of pellets.

5. Acknowledgments

The authors are grateful for the valuable financial support of Brazilian research funding agency CAPES and Embrapii, polo Vitória, ITV-Vale, proc. 2016-2.

6. References

1. Chen W, Biswas S, Roberts A, O'Shea J, Williams K. Abrasion wear resistance of wall lining materials in bins and chutes during iron ore mining. *Int J Miner Process.* 2017;167:42-8. <http://dx.doi.org/10.1016/j.minpro.2017.08.002>.
2. Ibrahim KM, Ibrahim MM. Heat Treatment in High Chromium White Cast Iron Ti Alloy. *J Metall.* 2014;2014:1-9. <http://dx.doi.org/10.1155/2014/856408>.
3. Karantzalis AE, Lekatou A, Diavati E. Effect of destabilization heat treatments on the microstructure of high-chromium cast iron: a microscopy examination approach. *J Mater Eng Perform.* 2009;18(8):1078-85. <http://dx.doi.org/10.1007/s11665-009-9353-6>.
4. Bedolla-Jacunde A, Arias L, Hernández B. Kinetics of secondary carbides precipitation in a high-chromium white iron. *J Mater Eng Perform.* 2003;12(4):371-82. <http://dx.doi.org/10.1361/105994903770342881>.
5. Tabrett CP, Sare IR. The effect of heat treatment on the abrasion resistance of alloy white irons. *Wear.* 1997;203-204:206-19. [http://dx.doi.org/10.1016/S0043-1648\(96\)07390-5](http://dx.doi.org/10.1016/S0043-1648(96)07390-5).
6. Wang J, Li C, Liu H, Yang H, Shen B, Gao S, et al. The precipitation and transformation of secondary carbides in a high chromium cast iron. *Mater Charact.* 2006;56(1):73-8. <http://dx.doi.org/10.1016/j.matchar.2005.10.002>.
7. Gasan H, Erturk F. Effects of a destabilization heat treatment on the microstructure and abrasive wear behavior of high-chromium white cast iron investigated using different characterization techniques. *Metall Mater Trans, A Phys Metall Mater Sci.* 2013;44(11):4993-5005. <http://dx.doi.org/10.1007/s11661-013-1851-3>.
8. Lai JP, Pan QL, Wang ZB, Cui HR, Wang XD, Gao ZZ. Effects of destabilization temperature on the microstructure and mechanical properties of high chromium cast iron. *J Mater Eng Perform.* 2017;26(10):4667-75. <http://dx.doi.org/10.1007/s11665-017-2943-9>.
9. Xu L, Vose C, StJohn D. Abrasive wear study of selected white cast irons as liner materials for the mining industry. *Wear.* 1993;162-164:820-32. [http://dx.doi.org/10.1016/0043-1648\(93\)90083-X](http://dx.doi.org/10.1016/0043-1648(93)90083-X).
10. Kirchgäßner M, Badisch E, Franek F. Behaviour of iron-based hardfacing alloys under abrasion and impact. *Wear.* 2008;265(5-6):772-9. <http://dx.doi.org/10.1016/j.wear.2008.01.004>.
11. American Society for Testing and Materials – ASTM. ASTM E-975: standard practice for X-ray determination of retained austenite in steel with near random crystallographic orientation. West Conshohocken: ASTM; 2013.
12. Ratia V, Miettunen I, Kuokkala VT. Surface deformation of steels in impact-abrasion: the effect of sample angle and test duration. *Wear.* 2013;301(1-2):94-101. <http://dx.doi.org/10.1016/j.wear.2013.01.006>.
13. Rocha DL. Influência da temperatura de desestabilização na resistência ao desgaste de um ferro fundido alto cromo [dissertation]. Vitória: Instituto Federal do Espírito Santo; 2019 [cited 2023 May 16]. Available from: <http://biblioteca.ifes.edu.br:8080/pergamumweb/vinculos/000017/000017bb.pdf>
14. Wilson RD, Hawk JA. Impeller wear impact-abrasive wear test. *Wear.* 1999;225-229:1248-57. [http://dx.doi.org/10.1016/S0043-1648\(99\)00046-0](http://dx.doi.org/10.1016/S0043-1648(99)00046-0).